

# Towards an explanation for the 30 Dor (LMC) Honeycomb nebula – the impact of recent observations and spectral analysis.

J. Meaburn<sup>1\*</sup>, M. P. Redman<sup>2</sup>, P. Boumis<sup>3</sup> and E. Harvey<sup>2</sup>

<sup>1</sup>*Jodrell Bank Centre for Astrophysics, University of Manchester, Manchester M13 9PL, UK.*

<sup>2</sup>*Centre for Astronomy, School of Physics, National University of Ireland Galway, University Road, Galway, Ireland.*

<sup>3</sup>*Institute of Astronomy & Astrophysics, National Observatory of Athens, I. Metaxa & V. Pavlou, GR-152 36 P. Penteli, Athens, Greece.*

Received; Accepted

## ABSTRACT

The unique Honeycomb nebula, most likely a peculiar supernova remnant, lies in 30 Doradus in the Large Magellanic Cloud. Due to its proximity to SN1987A, it has been serendipitously and intentionally observed at many wavelengths. Here, an optical spectral analysis of forbidden line ratios is performed in order to compare the Honeycomb high-speed gas with supernova remnants in the Galaxy and the LMC, with galactic Wolf–Rayet nebulae and with the optical line emission from the interaction zone of the SS433 microquasar and W50 supernova remnant system. An empirical spatiokinematic model of the images and spectra for the Honeycomb reveals that its striking appearance is most likely due to a fortuitous viewing angle. The Honeycomb nebula is more extended in soft X-ray emission and could in fact be a small part of the edge of a giant LMC shell revealed for the first time in this short wavelength domain. It is also suggested that a previously unnoticed region of optical emission may in fact be an extension of the Honeycomb around the edge of this giant shell. A secondary supernova explosion in the edge of a giant shell is considered for the creation of the Honeycomb nebula. A microquasar origin of the Honeycomb nebula as opposed to a simple supernova origin is also evaluated.

**Key words:** ISM: individual: Honeycomb nebula - ISM: supernova remnants - Magellanic clouds.

## 1 INTRODUCTION

The 30 Doradus nebula in the Large Magellanic Cloud (LMC) is the most massive and largest H II complex in the Local Group of galaxies. Its 300 pc diameter core and adjacent halo exists between two 1000 pc diameter supergiant filamentary shells (Meaburn 1979; 1980). The multitude of young massive stars scattered throughout this region identify it as a nursery of recent star formation consequently, the supernova (SN) rate is of particular interest. The explosion of SN1987A emphasised that these events are ongoing.

The SN rate in this nebular complex has been considered by several authors recently. In particular Lazendic, Dickel & Jones (2003) using high resolution optical, radio and X-ray imagery searched for young supernova remnants (SNRs) in its central 80 pc diameter region but came up with only four regions with high radio/H $\alpha$  ratios. However, two

of these were associated with young HII regions with young embedded stellar objects. Chu et al. (2004) then showed the remaining two SNR candidates to be dust clouds or obscured star forming regions. This leaves N157 along with the Honeycomb nebula (Wang 1992) as the only firm SNR candidates but many more young (1000 yr old) remnants are likely to be present but as yet undetected. This probability lead Meaburn (1984; 1988) to suggest that such remnants could be identified by the high-speed (200-300 km s<sup>-1</sup>) velocity ‘spikes’, with predominantly approaching radial velocities, that are present in the longslit position–velocity (pv) arrays of optical line profiles (e.g. see fig.3 of Meaburn 1988). Chu et al. (1994) suggested quite correctly that these are not necessarily diagnostic of SN activity because wind-blown shells, particularly around Wolf–Rayet (WR) stars can have similar extents in radial velocity. Maybe individual SNRs just become merged and combine with particle winds to drive the giant (50–100 pc diameter) shells found around the many OB-associations in the 300 pc diameter halo of 30 Doradus.

\* E-mail: jmeaburn@jb.man.ac.uk

However, it seemed worthwhile to investigate if optical line brightness ratios of only the high-speed component of the 30 Doradus radial velocity spikes could be used as a diagnostic of individual SN origin. This opportunity became viable for it was realised that in previous, separate observations of the Honeycomb nebula (Wang 1992), itself most likely of SN origin for it is a non-thermal radio source (Chu et al. 1995 though see Sect. 4.4 for a more radical alternative possibility), that one slit position for  $H\alpha$  and  $[N\ II]\ 6548\ \&\ 6584\ \text{\AA}$  longslit line profiles (Meaburn et al. 1993) matched, within the ‘seeing’ disk, the position for the  $[S\ II]\ 6717\ \&\ 6731\ \text{\AA}$  profiles (Redman et al. 1999). Sound diagnostic optical line ratios of the high-speed ionized gas therefore became accessible.

In the present paper these line ratios of the Honeycomb nebula’s high-speed gas are evaluated and they resemble those of LMC but not Galactic SNRs. The creation and structure of the strange, and possibly unique, Honeycomb nebula itself, is re-considered also aided by the most recent Chandra and other X-ray imagery plus Hubble Space Telescope (HST) and ESO New Technology Telescope (NTT) imagery. The impact of these results on an evaluation of the 30 Doradus SNe rate is also considered.

## 2 OBSERVATIONS

Due to its location in the vicinity of SN1987A, the Honeycomb nebula has been observed by XMM-Newton and Chandra in the X-ray regime and in narrow band optical imaging with the NTT. Figure 1(a) shows narrow band images of the Honeycomb in  $H\alpha$  plus  $[N\ II]\ 6548\ \&\ 6584\ \text{\AA}$ . Figure 1(b) is an  $[O\ III]\ 5007\ \text{\AA}$  image, in which the Honeycomb is seen more extensively. Figure 1(c) is a Chandra X-ray image of the source in which it can be seen that the spatial extent of the X-ray emission closely matches the optical emission. Part of the Honeycomb was also serendipitously observed at the very edge of the field by the Hubble Space Telescope (HST) as part of a project to detect light echos from SN1987A (Crofts 1988). These broad-band observations are of much lower sensitivity than the narrow-band ones in Figs. 1a–b but do show that the edges of the Honeycomb cells are not resolved even at the resolution of the HST. The edge widths to cell diameter ratios are remarkably  $\leq 0.01$ . (see Sect.4.2 and Fig. 7).

$H\alpha$  and  $[N\ II]\ 6548\ \&\ 6584\ \text{\AA}$  (Meaburn et al. 1993) and  $[S\ II]\ 6717\ \&\ 6731\ \text{\AA}$  (Redman et al. 1999) line profiles were obtained using the Manchester Echelle Spectrometer (MES; Meaburn et al. 1984) on the Anglo-Australian telescope along the same (within the one arcsec wide seeing disk) slit position (Fig. 2a). The position-velocity (pv) array of  $[S\ II]\ 6717\ \&\ 6731\ \text{\AA}$  profiles along this slit is shown in Fig. 2b. The atmospheric conditions were photometric in both cases. The details of these observations and their analyses are fully described in the respective papers and will not be repeated here.

## 3 OPTICAL LINE BRIGHTNESS RATIOS

The two MES long slit pv arrays of line profiles had been converted into absolute surface brightnesses

( $B\ \text{erg s}^{-1}\ \text{cm}^{-2}\ \text{sr}^{-1}\ \text{\AA}^{-1}$ ) using the spectra of standard stars. The brightnesses along the slit length of each of the five emission lines were obtained in the heliocentric radial velocity ranges of  $V_{\text{hel}} = 150\text{--}230\ \text{km s}^{-1}$  and  $240\text{--}300\ \text{km s}^{-1}$  using YTRACT in the STARLINK FIGARO suite of data reduction programmes. The example pv array in Fig. 2b reveals that the former velocity range contains only the high-speed Honeycomb features whereas the latter range contains the emission from predominantly the 30 Doradus host nebula. The peaks of the  $B$  values for all five lines in the  $150\text{--}230\ \text{km s}^{-1}$  range occurred at the positions marked 1-6 in Fig. 2b and each is coincident with a high-speed velocity ‘spike’ from the Honeycomb nebula. The  $\log_{10} [H\alpha / ([N\ II]\ 6548\ \&\ 6584\ \text{\AA})]$  versus  $\log_{10} [H\alpha / ([S\ II]\ 6716\ \&\ 6731\ \text{\AA})]$  brightness ratios for the high speed ‘spikes’ are shown in Fig. 3 for positions 1–6 as square dots. Similarly the  $[S\ II]\ 6716\ \&\ 6731\ \text{\AA}$  ratios  $I(\lambda\ 6717)/I(\lambda\ 6731)$  versus  $\log_{10} [H\alpha / ([N\ II]\ 6548\ \&\ 6584\ \text{\AA})]$  and  $\log_{10} [H\alpha / ([S\ II]\ 6716\ \&\ 6731\ \text{\AA})]$  ratios are shown in Figs 4 and 5 respectively. The mean ratios for the 30 Dor host nebula from the same data are marked in each of Figs 3–5 by a cross. All of these values are compared with the regions occupied by line ratios of Galactic SNRs, H II regions and planetary nebulae (PNe) as given in the diagnostic diagrams of Sabbadin, Minello & Bianchini (1977). The values for LMC SNRs (Payne, White & Filipovic 2008) are shown as diamonds. The large open circles and large black dots only in Fig. 3 are for the Galactic filamentary WR nebulae NGC 3199 and RCW 104 as given by Whitehead, Meaburn & Goudis (1988) and Goudis, Meaburn & Whitehead (1988) respectively. One black dot for RCW 104 is of particular interest for it is for a high speed knot. This is shown in Fig. 3 with an arrow attached to show its limiting ratio as  $[S\ II]\ 6717\ \&\ 6731\ \text{\AA}$  was not detected.

The uncertainties in the Honeycomb  $\log_{10} [H\alpha / ([N\ II]\ 6548\ \&\ 6584\ \text{\AA})]$ ,  $\log_{10} [H\alpha / ([S\ II]\ 6716\ \&\ 6731\ \text{\AA})]$  and  $I(\lambda\ 6717)/I(\lambda\ 6731)$  brightness ratios are  $\pm 0.04$ ,  $\pm 0.04$  and  $\pm 0.05$  respectively. Those for the brighter emission from the host 30 Doradus nebula are significantly smaller.

## 4 DISCUSSION

### 4.1 Line ratio diagnostics

The Honeycomb nebula is a non-thermal radio source and therefore most likely of SN origin (Chu et al. 1994; 1995) though see Sect. 4.4 for a more radical, but unlikely, possibility. However, it is striking that the positions of the line ratios of the Honeycomb high-speed gas, on the diagnostic diagrams in Figs. 3–5 match most closely those occupied by LMC but not Galactic SNRs. These positions are significantly away from those for Galactic SNRs before considering that the nitrogen abundance of the LMC is lower by a factor of 2 compared with that of the Galaxy (Russell & Dopita 1992). This could proportionally lower the  $[N\ II]\ 6584\ \text{\AA}$  brightness from the Honeycomb nebulosity and move line ratios closer to the Galactic SNR zones in Figs. 3 & 5.

Furthermore, ratios for the high speed Honeycomb gas bear no resemblance to those of the two WR nebulae considered here (Fig. 3) even when Galactic and LMC abundance differences are taken into account. Even the high-speed component of the Galactic WR nebula, RCW 104, is far removed

from the Honeycomb zone. When determining the SN rate for the halo of the 30 Doradus nebula from the number of high-speed velocity spikes over the region (Meaburn 1984; 1988) any confusion with those of WR origin is easily clarified by the relative positions of their line ratios on diagnostic diagrams.

## 4.2 Modelling kinematics and morphology

The SHAPE code of Steffen (see Steffen, Holloway & Pedlar 1996 for its initial use and Steffen & López 2006) permits the actual structure and kinematics of a nebula to be deduced from the imagery (Fig. 1 a–b) and long-slit pv arrays (such as that shown in Fig. 2b). No consideration of emission mechanisms or of the dynamics is involved here but the spatio-kinematic modelling is useful to investigate how critical the viewing angle is to the unique Honeycomb morphology.

The Honeycomb was modelled as a set of cylinders with equal length and diameter (since the Rayleigh–Taylor instability, for example, tends to grow most rapidly for those modes of order of the thickness of the disturbed layer). The edges of some of the Honeycomb cells are visible in archive HST images yet are unresolved. The edge widths to cell diameter ratios are  $\leq 0.01$ .

The Chandra images (eg. Fig. 1c) are of comparable resolution to the size of the cells but do seem more indicative of emission from the centre of each cell rather than poorly resolved boundary layers. A simple model would then be of hot X-ray emitting gas venting through gaps in a pre-existing shell or layer of gas and accelerating the preexisting material in a boundary layer at the cell edges. Therefore, the Honeycomb cells were modelled with SHAPE as a series of very thin, nested optically emitting cylinders, with each cylinder inwards having an increasing characteristic velocity. The blueshifted velocity spikes (eg. Fig. 2b) then result from this range of velocities being simultaneously present within the unresolved edges of the Honeycomb cells. While the Honeycomb morphology and kinematics can be reproduced in such an empirical model, it should be stressed that it does not describe the radiation emission or hydrodynamics of the system.

More interesting perhaps is to examine what happens when the model system described above is viewed from a different angle. Figs. 6a–c show that the circular cells, when viewed from increasing viewing angle, rapidly overlap and become blended into arcs and knots, somewhat reminiscent of the tangled filamentary structure that is commonly seen in optical emission lines toward the edges of SNRs. Similarly, the striking velocity spikes characteristic of the Honeycomb blend into more confused and diffuse emission on the pv array. If the material forming the cell edges is being continually entrained and eroded then the extreme thinness of the cell edges suggests that the uniqueness of the Honeycomb could simply be due to it being a short-lived structure viewed from a fortuitous angle. The low cell edge width to diameter ratio of the most prominent cell is clear in the HST image in Fig. 7 and should be compared to its synthetic image in Fig. 6a.

However, the Honeycomb may not be being viewed exactly in the plane of the sky. The individual cells are almost all distinctly brighter on their western sides which is easily reproduced by the SHAPE code if they are viewed at a small angle to the line of sight. Furthermore, there are redshifted

velocity spikes present in the Honeycomb that are not explained by the empirical model above though see possible explanation in Sect. 4.3.

## 4.3 A SN explosion in an expanding LMC giant shell

It was thought that the Honeycomb appearance and the pv arrays across the nebula could only be produced as a secondary SN blast wave encountered clumps of material in the nearside of a preceding expanding shell (e.g. see fig. 3 of Redman et al. 1999). This interpretation can certainly explain the nearly circular features in the imagery and the predominance of approaching velocity ‘spikes’ in the pv arrays of line profiles which are coincident with the edges of the sub-shells in the nebular image.

However, it fails to explain the elongated, three ridge structure that is particularly evident in the Chandra X-ray image in Fig. 1c and the fact that positive velocity spikes occur over the most westerly ridge of Honeycomb shells which are most apparent in the [O III] 5007 Å image in Fig. 1b. Another possibility therefore is that such a secondary SN explosion has occurred in the edge of a preceding giant LMC shell but now viewed tangentially to this previous feature (see Fig. 8). The three ridges of secondary Honeycomb shells could then be in folds of the surface of the original shell. Direct, but partial, evidence for the existence of this preceding  $\approx 8'$  ( $\equiv 130$  pc) diameter giant shell centred on RA 05h 36m 30s DEC  $-69^\circ 19'$  (J 2000) can be seen in the X-ray imagery in fig. 5 of Dennerl et al. (2001), fig 1l of Dunne, Points & Chu (2001) and fig. 2 of Smith & Wang (2004). The Honeycomb nebula forms a small part of its western edge but only a northern ridge is clearly detected at X-ray wavelengths. The X-ray image of Dennerl et al. (2001) shows a bright feature at the Honeycomb location that also clearly extends in an arc to the northeast. This extended X-ray feature is compared in Fig. 9 to the area of the images in Figs. 1a–c. Strangely, fainter Honeycomb-like features are also present in optical images along parts of this ridge mostly outside the area of Figs 1a–c (but see top-left of Fig.1a) but as yet no line profiles have been obtained from them to confirm their Honeycomb nature.

## 4.4 A microquasar origin

The unusual, and possibly unique, morphology and kinematics of the Honeycomb nebula warrants the consideration of a more radical possibility than given in Sect. 4.3 for its origin. Could it be the manifestation of the collision of a precessing relativistic jet emitted by a binary microquasar similar to SS 433 (for a review see Fabrika 2004), Cygnus X–1 (Russell et al. 2007), IC 342 X–1 (Feng & Kaaret 2008) and that in the galaxy NGC 7793 (Soria et al. 2009)? Non-thermal radio emission as seen emanating from the Honeycomb nebula would also be expected in this interaction zone between the jet and the ambient gas.

The eight hard X-ray point sources found by Haberl et al. (2001) in the vicinity of the Honeycomb nebula, could be candidates for the origin of such a jet. Although Haberl et al. (2001) strongly favour background active galactic nuclei for the origin of these point, hard X-ray sources, they do not completely rule out the microquasar possibility in all cases.

The faintest of these eight point sources (Source 1 of Haberl et al. 2001) has no measured spectral index and can be seen in their fig. 5 to be well placed with respect to the Honeycomb nebula if such a microquasar mechanism is occurring and if this nebula is on the western edge of an elongated structure with this source central. A much fainter candidate is the marginally detected point source arrowed in Fig. 9 but seen more clearly in fig. 5 of Haberl et al. (2001) though not listed by these authors. This is towards the centre of the more spherical giant shell proposed here to have the Honeycomb nebula at its edge.

However, it is interesting that the optical line ratios for the Galactic SS 433/W50 nebulosity (Boumis et al. 2007) when placed into the diagnostic diagrams shown in Figs. 3–5 bear no resemblance to the Honeycomb ratios or any other phenomena except Galactic planetary nebulae. Perhaps, the X-rays from the SS 433 jet are radiatively ionizing the processed material of the W50 SNR envelope. Furthermore, the different X-ray properties of the Honeycomb Nebula and W50 do not support a microquasar origin for the former. Even though these points argue against a microquasar origin for the Honeycomb nebula it will still be worthwhile to see if any stars within the error boxes of the two point X-ray sources in Fig. 9 have microquasar characteristics.

## 5 CONCLUSIONS

The optical line ratios of the high-speed Honeycomb nebula confirm its most likely SNR origin.

The velocity spikes on pv arrays of longslit line profiles found over the rest of the halo of 30 Doradus can be identified as of young SNR origin if they also occupy the LMC SNR zone on such diagrams. In this way they can be distinguished from high-speed WR shells.

The circular structures of the Honeycomb gas and their corresponding approaching and receding, highly collimated, flows can be modelled as a young SNR in the edge of a larger and preceding giant shell. The appearance and kinematics of the separate Honeycomb cells is strongly dependent on viewing angle i.e. they are only apparent if the cell walls are viewed along their cylindrical axes.

An alternative view that this unique nebula could be the consequence of a microquasar jet (similar to that from SS 433) is shown from comparative optical line ratios, and by other arguments, to be highly unlikely but not completely dismissed as there are two point X-ray sources in its vicinity, and because it is such a strange object.

The positions of the line ratios of the SS 433/W 50 interaction nebulosity on the diagnostic diagrams are remarkable in their own right.

## REFERENCES

- Boumis, P., Meaburn, J., Alikakos, J., Redman, M. P., Akras, S., Mavromatakis, F., López, J. A., Caulet, A. & Goudis, C. D., 2007, *MNRAS*, 381, 308.
- Chu, Y. H., Wakker, B., MacLow, M. M. & Garcia-Segura, G., 1994, *AJ*, 108, 1696.
- Chu, Y. H., Dickel, J. R., Staveley-Smith, L., Osterberg, J. & Smith, R. C., 1995, *AJ*, 109, 1729.
- Chu, Y. H., Gruendl, R. A., Chen, C. H. R., Lazendic, J. S. & Dickel, J. R., 2004, *ApJ*, 615, 727.
- Crotts, A. P. S., 1988, *ApJ*, 333, L51.
- Dennerl, K., Haber, F., Aschenbach, B. et al., 2001, *A&A*, 365, L202.
- Dunne, B. C., Points, S. D. & Chu, Y. H., 2001, *ApJS*, 136, 119.
- Fabrika, S., 2004, *ApSph Rev.*, 12, 1.
- Feng, H. & Kaaret, P., 2008, *ApJ*, 675, 1067.
- Goudis, C. D., Meaburn, J. & Whitehead, M. J., 1988, *A&A*, 191, 341.
- Haberl, F., Denner, K., Filipovic, M. D., Aschenbach, B., Pietsch, W. & Trumper, J., 2001, *A&A*, 365, L211.
- Lazendic, J. S., Dickel, J. R. & Jones, P. A., 2003, *ApJ*, 596, 287.
- Meaburn, J., 1979, *A&A*, 75, 127
- Meaburn, J., 1980, *MNRAS*, 192, 365
- Meaburn, J., Blundell, B., Carling, R., Gregory, D. E., Keir, D. F. & Wynne C. G., 1984, *MNRAS*, 210, 463.
- Meaburn, J., 1984, *MNRAS*, 211, 521
- Meaburn, J., 1988, *MNRAS*, 235, 375.
- Meaburn, J. Wang, L., Palmer, J. & López, J. A., 1993, *MNRAS*, 263, L6.
- Meaburn, J., López, J. A., Steffen, W., Graham, M.F. & Holloway, A.J., 1993, *ApJ*, 130, 2303.
- Payne, J. L., White, G. L. & Filipovic, M. D., 2008, *MNRAS*, 383, 1175.
- Redman, M. P., Al-Mostafa, Z. A., Meaburn, J., Bryce, M. & Dyson, J. E., 1999, *A&A*, 345, 943.
- Russell, S. & Dopita, M. A., 1992, *ApJ*, 384, 508.
- Russel, D. M., Fender, R. P., Gallo, E. & Kaiser C. R., 2007, *MNRAS*, 376, 1341.
- Sabbadin, F., Minello, S. & Bianchini, A., 1977, *A&A*, 60, 147.
- Smith, D. A. & Wang, Q. D., 2004, *ApJ*, 611, 881.
- Steffen, W., Holloway, A. J. & Pedlar, A., 1996, *MNRAS*, 282, 1203.
- Steffen, W. & López, J. A., 2006, *Rev. Mex. AA.*, 42, 99.
- Soria, R., Pakull, M., Broderick, J. Corbel, S. & Motch, C., 2009, *Proc. of “X-ray Astronomy 2009”*, eds. A. Comastri et al., in press (astro-ph.HE, arXiv:0912.2732v1).
- Pal, S., Chakrabarti, S. K., Kraus, A. & Mandal, S., 2006, *Bull. Astr. Soc. India*, 34, 1.
- Wang, L., 1992, *ESO Messenger*, No. 69, 34.
- Whitehead, M. J., Meaburn, J. & Goudis, C. D., 1988, *A&A*, 196, 261.

## ACKNOWLEDGMENTS

We thank Wolfgang Steffen for help using the SHAPE coded and Ravi Sankrit for past useful discussions and advice on Chandra data.

This paper has been typeset from a  $\text{\TeX}$ / $\text{\LaTeX}$  file prepared by the author.

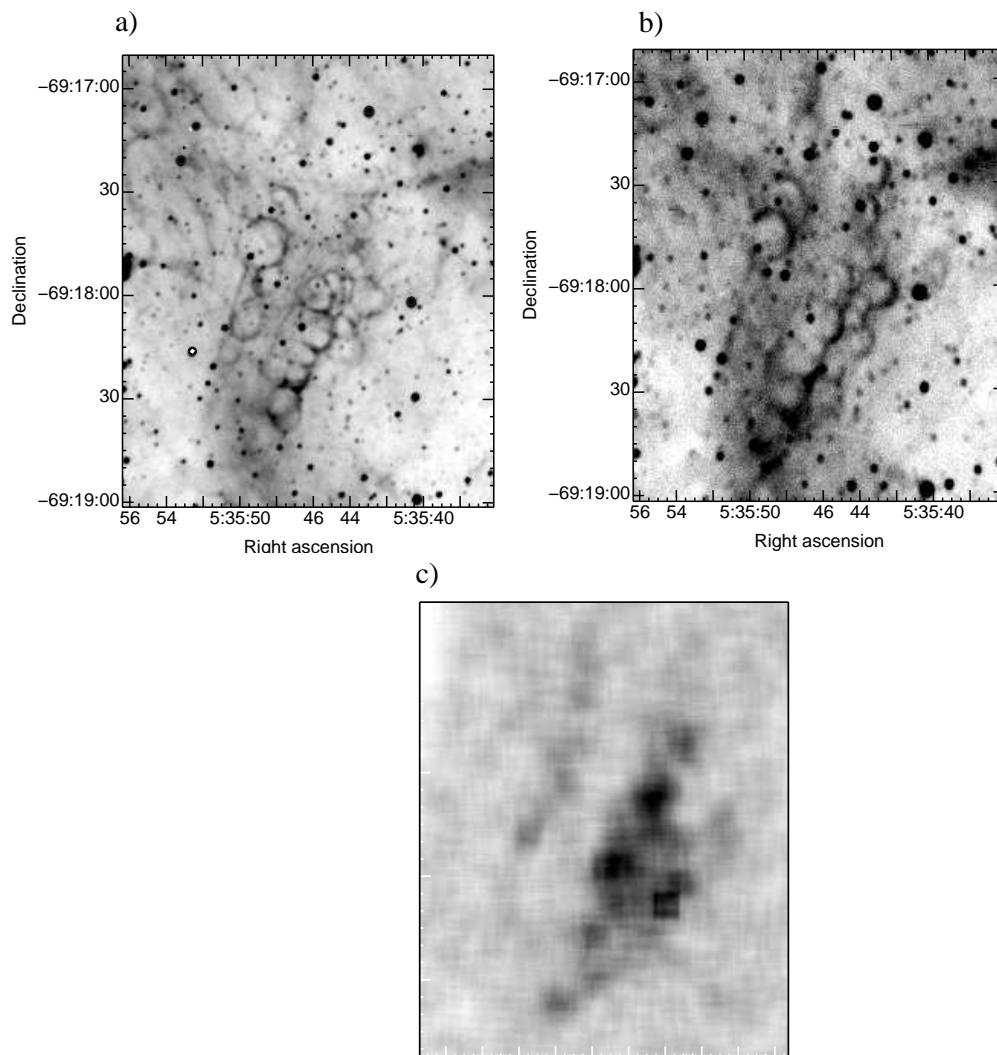
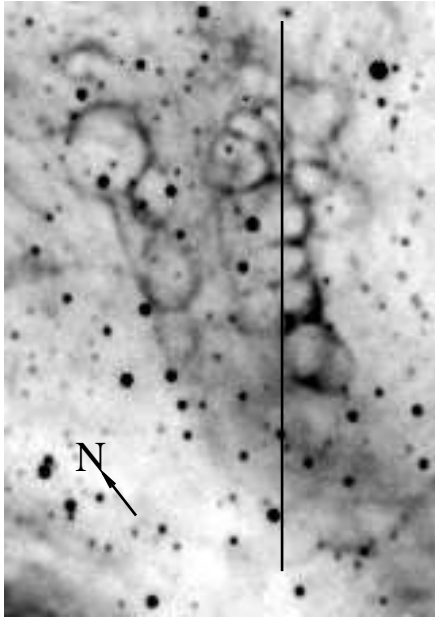


**Figure 1.** The a)  $H\alpha+[N\ II]$  6548 & 6584 Å and b)  $[O\ III]$  5007 Å images of the Honeycomb nebula are compared with c) the Chandra X-ray image. All are for the same area of the sky. (J2000 coords).

a)



b)

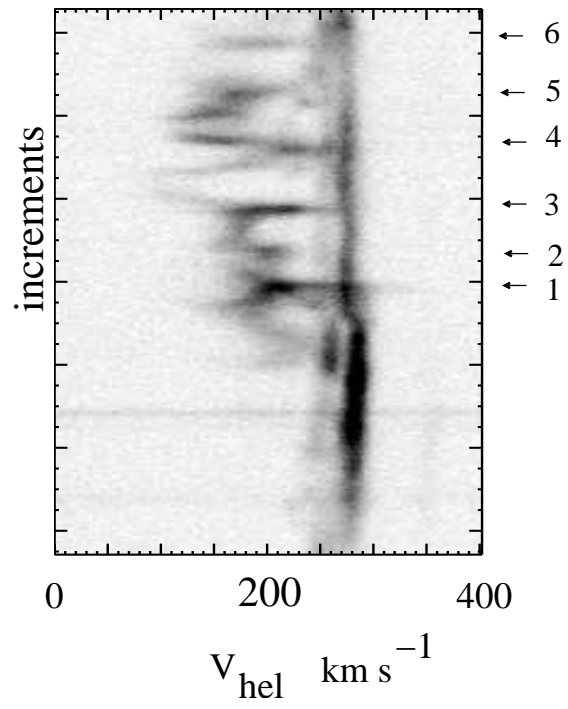


**Figure 2.** a) The position of part of the longslit is shown against the  $H\alpha + [N II] 6548 \text{ \AA}$  &  $6584 \text{ \AA}$  image of the Honeycomb nebula and compared in b) with the pv array of  $[S II] 6717 \text{ \AA}$  &  $6731 \text{ \AA}$  profiles along this same length. The positions 1-6 coincident with negative velocity 'spikes' where line ratios were measured are also indicated.

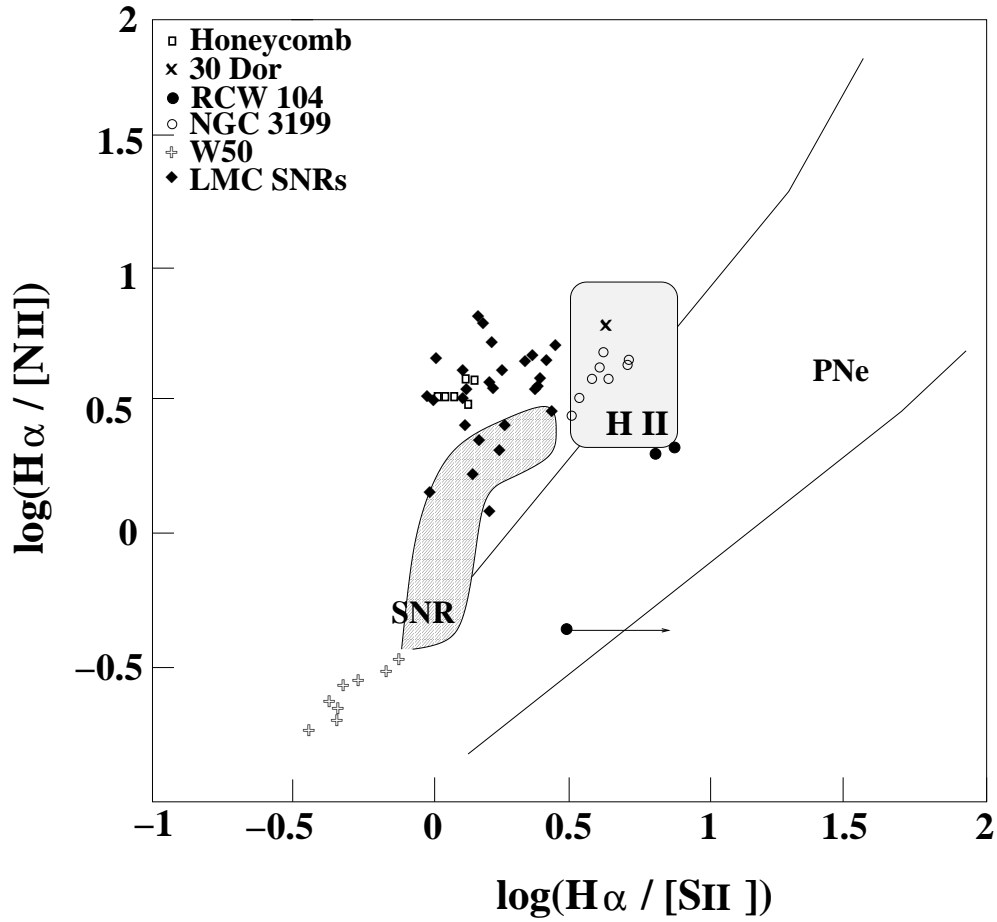


**Figure 3.** The six line intensity ratios (square dots) measured for positions 1–6 (Fig. 2b) for the high speed components in the Honeycomb line profiles are compared with the areas of this diagnostic diagram occupied by galactic SNRs, H II regions and planetary nebulae. The mean of the line ratios for 30 Doradus in the same vicinity is marked as a cross. Also shown are line ratios for two galactic Wolf–Rayet nebulae RCW 104 and NGC 3199. The large dot with an arrow is for the high-speed gas in RCW 104 and the arrow indicates that the [S II] 6717 & 6731 Å lines were not detected. All other WR values are for the filamentary features. The values for LMC SNRs are shown as diamonds. The ratios for the W 50 nebula generated by the microquasar, SS 433, are shown by plus signs.



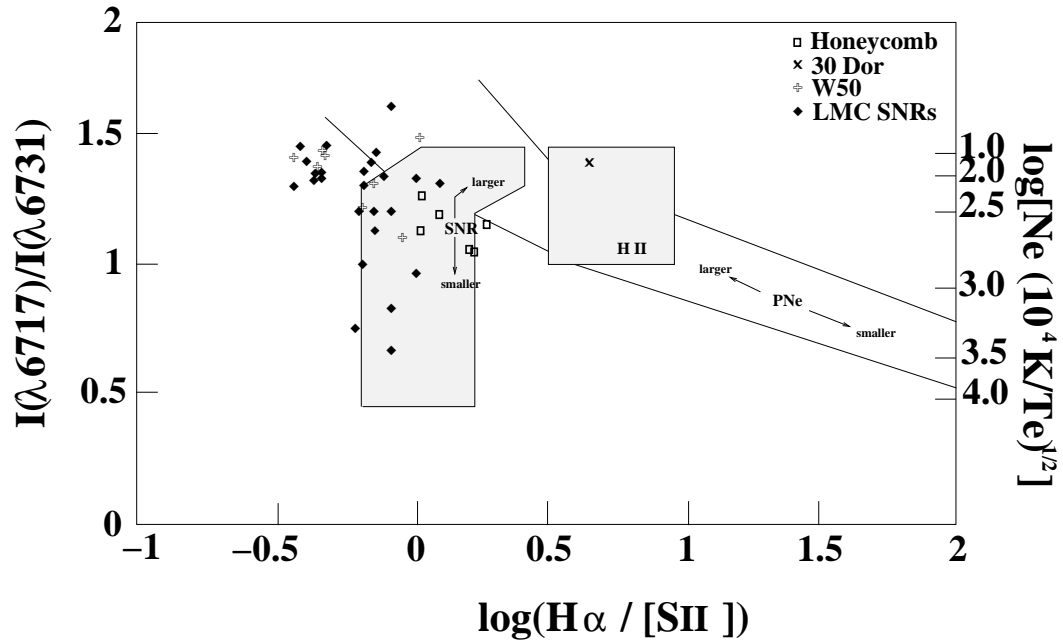


Figure 4. Similar diagnostic diagram to that in Fig. 3 but no values for the WR nebulae were available.

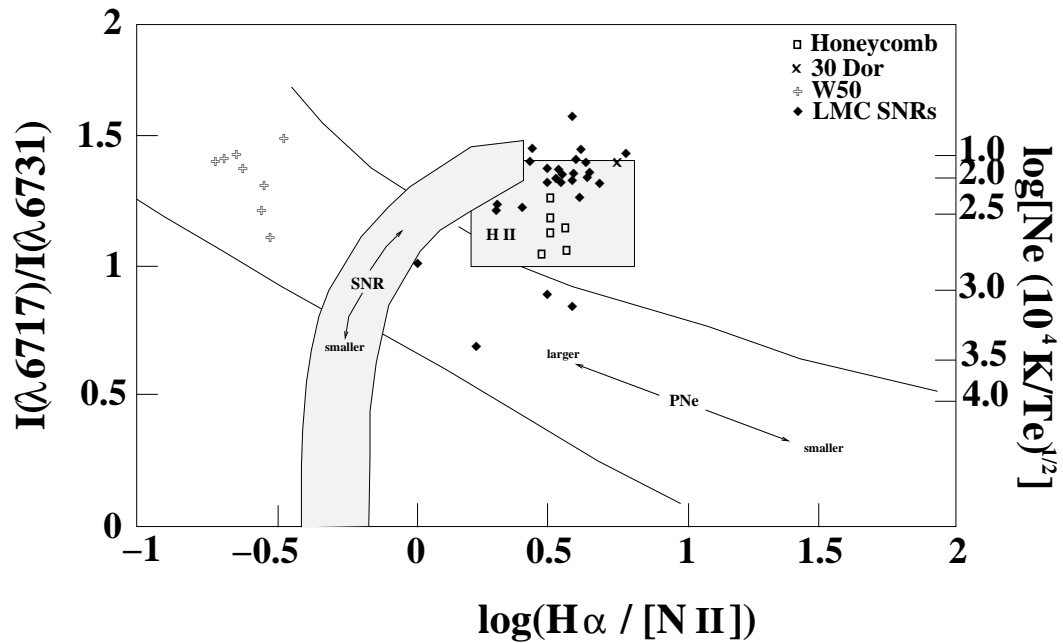
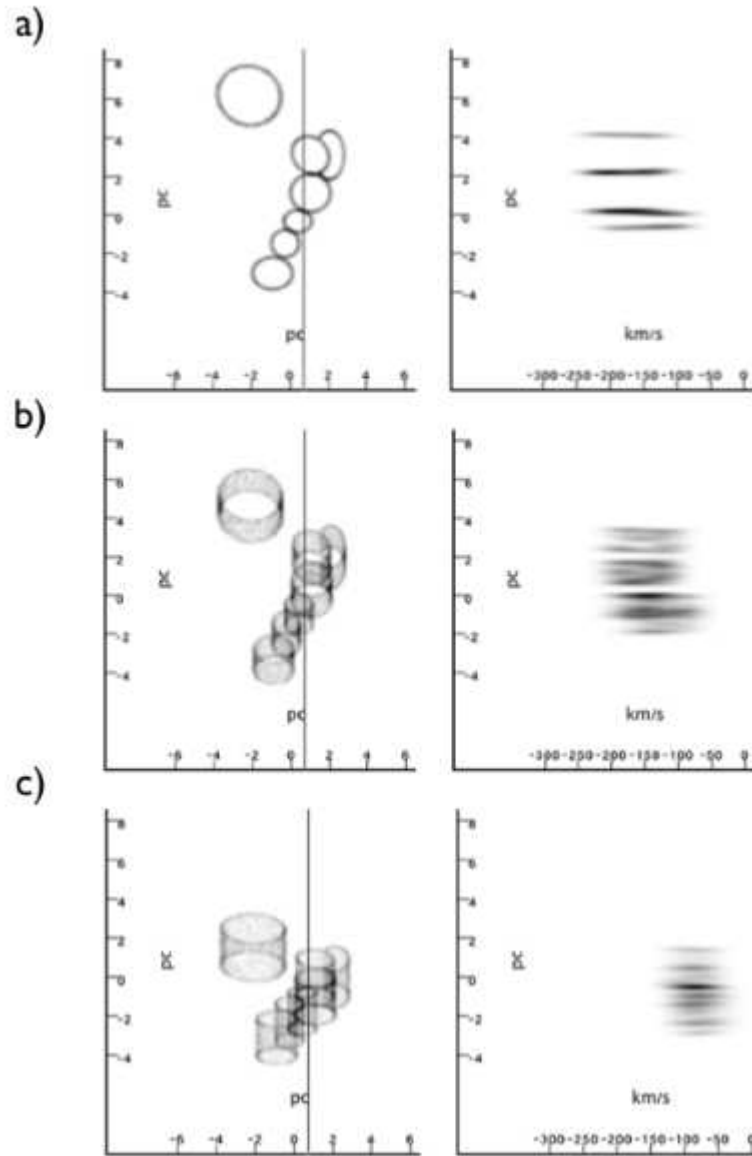
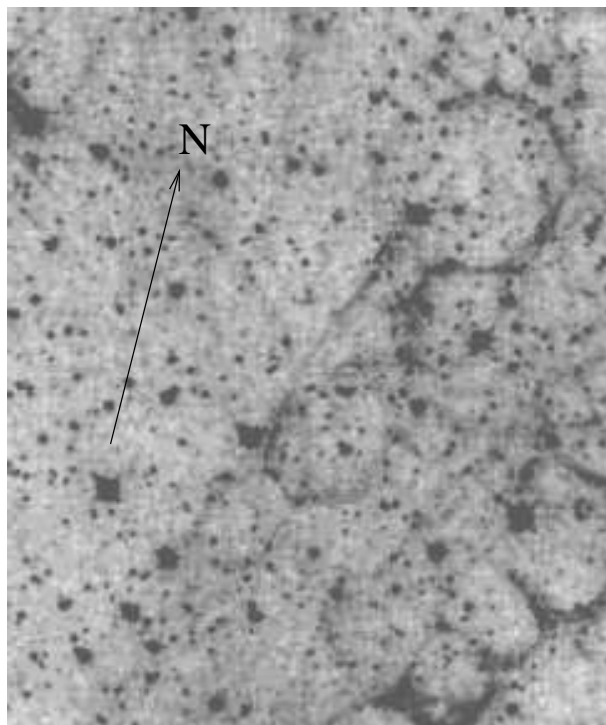


Figure 5. Similar diagnostic diagram to that in Fig. 3 but again (as for Fig. 4) no values for the WR nebulae were available.



**Figure 6.** a) SHAPE code model of the Honeycomb as a set of cylinders viewed end-on. The image is on the left and the synthetic pv array on the right for the slit position marked in Fig. 2a. Sharp ‘velocity spikes’ are generated. The synthetic images and pv arrays in (b) and (c) are for the same model as in Figure 6a but viewed at angles of 45 and 60 degrees respectively. The Honeycomb structure loses coherence and the velocity spikes become shortened and blended. The radial velocity scale is with respect to systemic value for this region of the 30 Doradus halo.



**Figure 7.** The broadband HST (675 nm) image of part of the field shown in Fig.1 a-c. The low edge width to diameter ratio of the most prominent Honeycomb shell (top right) should be compared to its synthetic image in Fig. 6a.

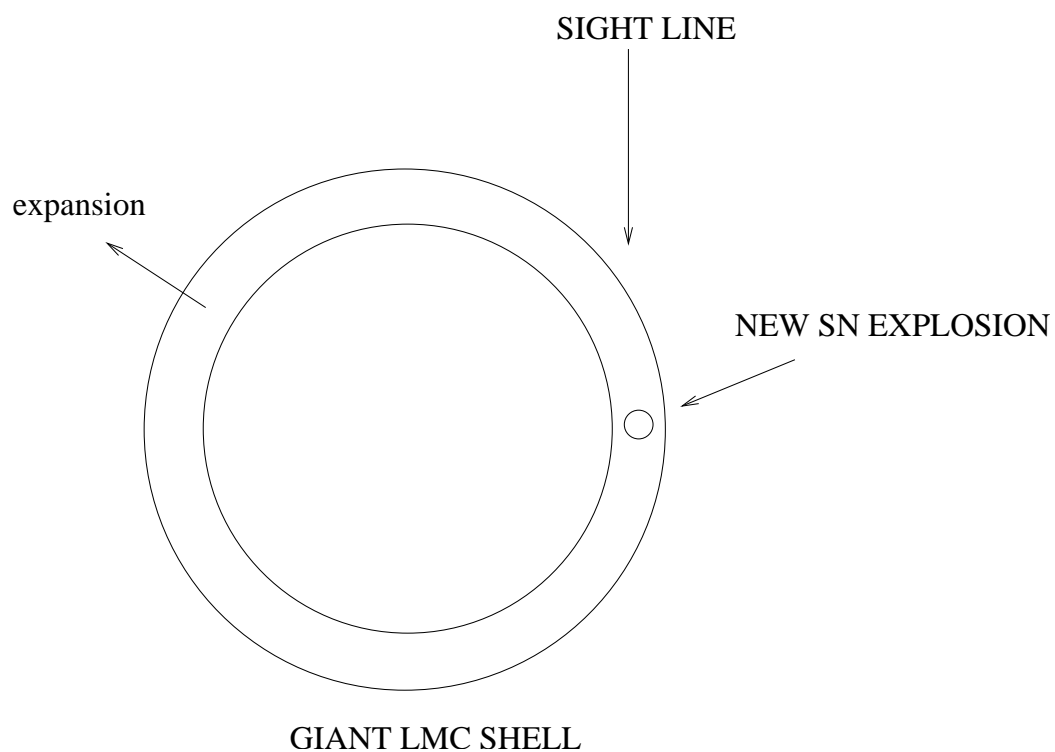


**Figure 8.** The positive and negative high-speed velocity spikes in pv arrays can be generated by a young SNR in the edge of an LMC giant shell. A more realistic depiction would have clumpy material in the giant shell and it to have a more irregular structure than sketched here. Positive and negative flows in the cylindrical cells around clumps would be seen along the sight-line marked here.

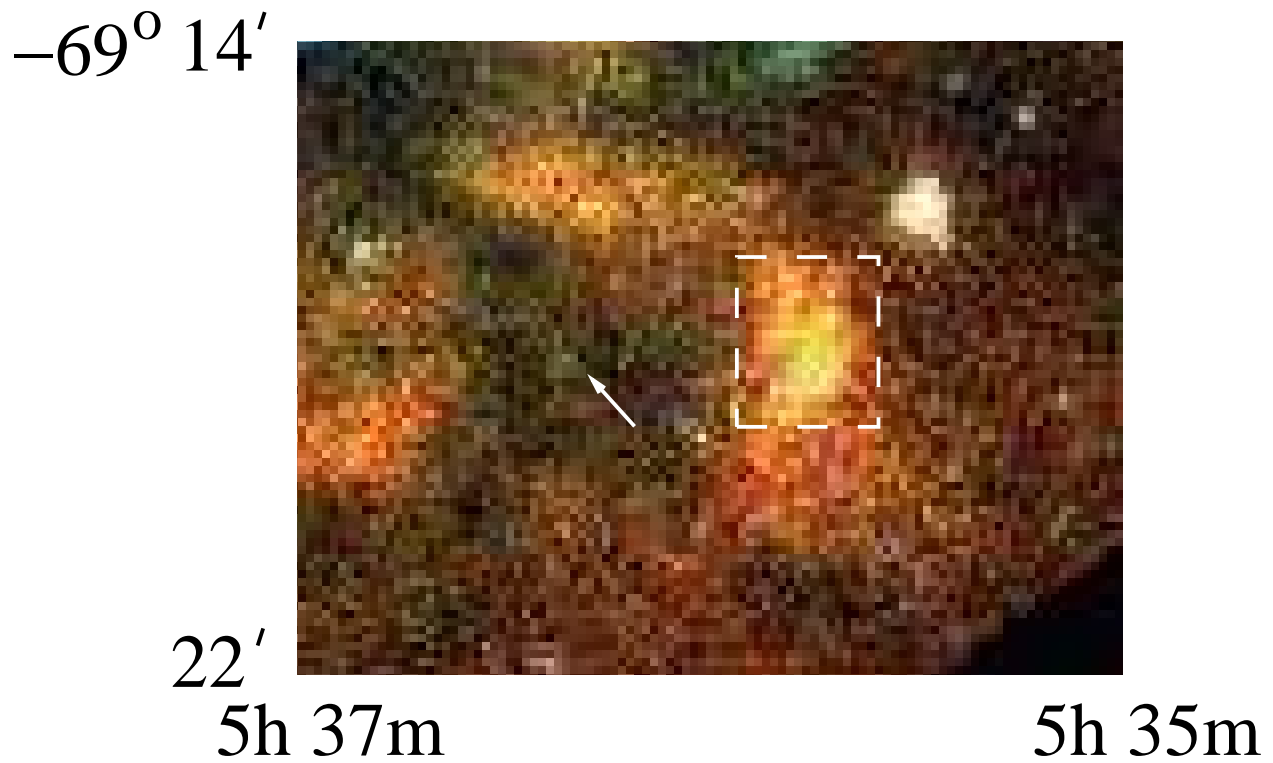


**Figure 9.** The area of Figs.1a–c is shown as a dashed box against a subset of the XMM X-ray image from Dennerl et al. (2001). Softer X-rays become orange in this presentation and hard blue. SN1987A is the bright source towards the top right and the point X-ray source number 1 of Haberl et al. (2001) is towards the top left (J2000 coords). An arrow points to a marginally detected point source which is more apparent in the original image of Dennerl et al. (2001)